Design and Characterisation of a Real Time Proton and Carbon Ion Radiography system based on scintillating optical fibres

D. Lo Presti[a,b,*], D. L. Bonanno[b], F. Longhitano[b], D. G. Bongiovanni[b], G. V. Russo[a], E. Leonora[b], N. Randazzo[b], S. Reito[b], V. Sipala[c,d], G. Gallo[a,b]

[a] *Department of Physics and Astronomy, University of Catania, Italy*
[b] *Istituto Nazionale di Fisica Nucleare (INFN), Sezione Catania, Italy*
[c] *University of Sassari, Sassari, Italy*
[d] *Istituto Nazionale di Fisica Nucleare (INFN), Sezione di Cagliari, Italy*

Abstract

This paper describes the design and characterization of a charged particle imaging system composed of a position sensitive detector and residual range detector. The position detector consists of two identical overlying and orthogonal planes each of which consists of two layers of pre-aligned and juxtaposed scintillating fibres. The 500 µm square section fibres are optically coupled to two Silicon Photomultiplier arrays using a channel reduction system patented by the Istituto Nazionale di Fisica Nucleare. The residual range detector consists of sixty parallel layers of the same fibres used in the position detector each of which is optically coupled to a Silicon Photomultiplier array by wavelength shifting fibres. The sensitive area of the two detectors is 9×9 cm^2. Characterising the position sensitive and the residual range detectors to reconstruct the radiography, is fundamental to validating the detectors' designs. The proton radiography of a calibrated target in imaging conditions is presented. The spatial resolution of the position sensitive detector is about 150 µm and the range resolution is about 170 µm. The performance of the prototypes were tested at CATANA proton therapy facility (Laboratori Nazionali del Sud, INFN, Catania) with energy up to 58 MeV and rate of about 10^6 particles per second. The comparison

*Corresponding author
Email address: domenico.lopresti@ct.infn.it (D. Lo Presti)

between the simulations and measurements confirms the validity of this system.

Keywords: Real-time proton radiography, Optical detector read-out strategy, Proton imaging, Scintillating optical fibres

---

1. Introduction

Cutting-edge research in the treatment of tumours is increasingly oriented towards hadron therapy, one of the most effective techniques of external radiation therapy that uses beams of charged particles, such as protons and carbon ions with energies up to 400 MeV/u. This technique helps destroy tumour cells precisely, while leaving the surrounding healthy tissues almost intact. In radiotherapy, the main advantages of heavy charged particle beams are achieved with accurate information on the stopping power of used particles. Only real-time precise quality control of the beam together with the best possible knowledge of the dose distribution, verification of the treatment plans (TPS, Treatment Planning System), and patient positioning provides the highest degree of therapy precision [1, 2]. Several technologies have produced detectors consisting of a position detector and a particle residual range detector. These systems were developed to accurately carry out parts of the following tasks:

- High resolution imaging;
- High resolution residual range measurement;
- Large sensitive area;
- Low number of read-out channels;
- High rate beam compliance.

This paper discusses the design and characterization of an innovative prototype (PREDATE, Particle Residual Energy Detector And Tracker Enhancement) of a charged particle imaging system for charged particle radiography based on 500 µm square section optical scintillating fibres (SciFi). This system

consists of two parts: a position sensitive detector (QBeRT, Qualification of Beam Real Time) and a particle Residual Range Detector (RRD).

The PREDATE prototype has innovative features which distinguish it from other similar devices: i) it is the only particle imaging system to date in which the RRD is made of scintillating fibres; ii) QBeRT uses a patented read-out channel reduction system which significantly reduces the complexity of the electronics needed to acquire signals in a Position Sensitive Detector (PSD).

The prototypes' performance was measured in beam tests at the CATANA proton therapy facility (Laboratori Nazionali del Sud, INFN, Catania) with energies up to 58 MeV, the validity of the results prompting INFN to file a patent application for the device [3].

The implemented architectures are thought to be modular and scalable. It is possible to obtain a large area detector (up to 40×40 cm^2) covering a range of up to 250 MeV protons with high spatial resolution (up to 150 µm) and high range resolution (up to 170 µm).

2. PREDATE particle imaging system

The research on devices for proton imaging is increasingly oriented towards the class of proton-tracking systems [4] which combines two types of detectors with distinct functions: a Position Sensitive Detector (PSD) and a particle Residual Range Detector (RRD). The PREDATE project, funded by the INFN regarding project IRPT (Innovative Research in Radio Therapy), has the ultimate goal of developing a real-time proton imaging system [5]. The layout of the final system is shown in figure 1. A PSD (QBeRT) measures the entry position for each particle passing through it, while the RRD measures its energy. The light signal produced by the particles passing through the fibres is collected by an SiPM (Silicon PhotoMultiplier) optically coupled to them. In the case of the PSD, applying a channel reduction system significantly reduces the number of read-out channels. The front-end electronic chain and high-speed data acquisition system, custom designed and built, can acquire sufficient events for

a radiography in a few minutes. The research covered the design, construction and characterization of the latest prototypes for the PSD and the RRD. The performance of these prototypes was tested at CATANA. The subsequent data analysis supported by accurate Monte Carlo simulations of the system provided the first radiographic image obtained with this system.

3. The QBeRT Position Sensitive Detector

QBeRT is the latest development of earlier prototypes developed in the OFF-SET (Optical Fibre Folded Scintillating Extended Tracker) project [6]. The QBeRT prototype has a sensitive area of 9×9 cm^2 consisting of four layers of 160 fibres each coated with white Extra Mural Absorber (EMA). We used 500 µm square section SciFi. A front view of the detector is shown in figure 2. In detail, each single layer consists of four SciFi ribbons of 40 fibres each. The ribbons are optically isolated from each other by means of 220 µm thick black

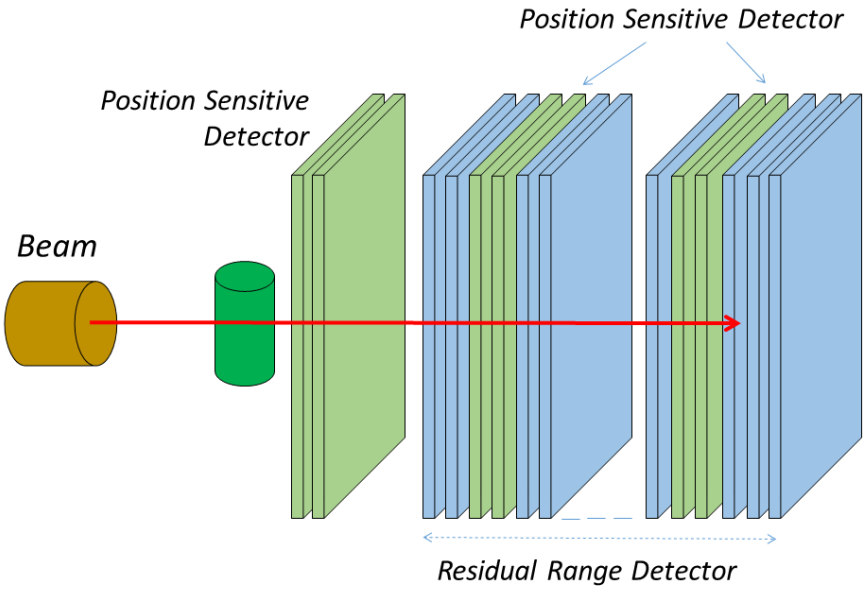

Figure 1: The layout of PREDATE detector. It consists of a Position Sensitive Detector (PSD) and a Residual Range Detector [6].

adhesive tape. This solution was adopted to eliminate the cross-talk between adjacent ribbons and between the superimposed layers of fibres. The use of EMA coated SciFi eliminated the cross-talk between individual fibres. The four layers are arranged to form two identical planes each consisting of two layers of aligned fibres called the X and Y layers. Particles crossing the PSD's sensitive area lose energy in the SciFi. This energy is absorbed and partially re-emitted as visible light in the fibre cores which is made of scintillating material. The re-emission occurs in an isotropic manner; therefore, only a fraction of the emitted light is channelled and travels along the fibre towards the photo-detectors. To detect where particles cross the sensitive area, they must deposit enough energy in all four SciFi layers. When they do, their impact coordinates can be measured with a resolution of about 150 µm.

The scintillation light channelled along the fibre reaches the light sensor which converts it into an electrical signal. In previous OFFSET prototypes, multi-anode PhotoMultipliers (psPM, position sensitive photomultiplier) were used. Due to different operating conditions with higher light levels, in the QbeRT detector the psPMs were replaced with SiPM arrays. Applying the patented channel reduction system reduced the number of read-out channel by a factor 5 [7]. The electrical signal produced by the sensor is processed by an electronic front-end and, subsequently, by data acquisition hardware. The acquired data can be processed and displayed in real time by a PC and stored. The choice of 500 µm square cross-section SciFi is a compromise between the resolution that can be achieved and the amount of light generated in the fibres. For any position sensitive digital detector, the pitch, p, between two adjacent sensing elements determines (a priori) spatial resolution. Since the differences between the measured and real positions have a Gaussian distribution, the spatial resolution is equal to the pitch divided by $\sqrt{12}$ [8]. Then, the maximum attainable spatial resolution with the 500 µm pitch is 144 µm. Better resolution can be obtained using narrower fibres, but the particle path length for scintillation would decrease and with it the amount of light produced in the fibres. Attenuation length is fundamental to the feasibility of a tracker made of

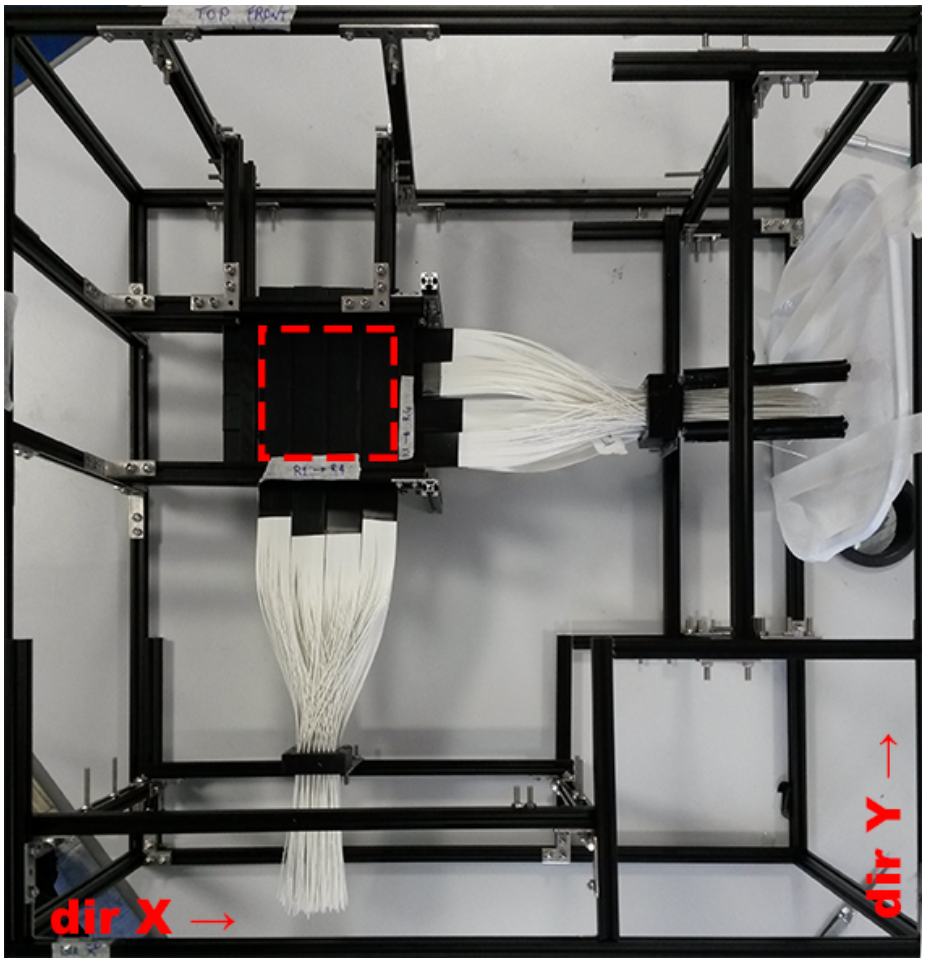

Figure 2: Front view of QBeRT detector during the assembly phases. The dashed red box highlights the sensitive area of the detector.

SciFi. In fact, the scintillation light channelled into the fibres must arrive at the photo-sensor in sufficient quantity to be detected. The manufacturer reports an attenuation length of $\lambda = 2.7\,\mathrm{m}$ for 1 mm round BCF-12. From this value, it is not possible to extrapolate the characteristics of a different fibre diameter and/or cross-section. The OFFSET collaboration conducted a specific study on the attenuation length of the selected fibres [6, 9]. As reported in [6], the attenuation length measured for the BCF-12 fibres with a 500 µm square cross-

section is about 1 m. Moreover, taking into account the fibre length necessary to produce the light sensor optical coupling, the widest sensitive area of such a detector was calculated to be about 45×45 cm^2. The QBeRT's sensitive area is smaller with an overall length of SciFi from the SiPM to the opposite end of the sensitive area being about 40 cm.

Each of the four QBeRT layers consists of 160 fibres, that is 640 optical channels. The read-out channels reduction system reduces this channel number, without any data loss on position information and since read-outs can now be done in time coincidence they are practically immune to noise, without increasing the complexity of the system. Note that to detect a particle, it must release energy in both planes. In the prototype, read-outs occur in time coincidence between the two layers of fibres for each plane. With a classical read-out system 640 channels are used, whereas the channel reduction system can read the signal from the whole tracker with only 112 channels (less than a fifth). Each of the 56 channels per plane is optically coupled to one of the 64 channels in the SiPM array.

A diagram of the channel reduction system for a position sensitive detector composed of 16 by 16 fibres is shown in figure 3. The star marks the crossing point of a particle in the sensitive area which consists of two superimposed fibre layers. The coordinates of the crossing point are given by:

$$\mathbf{Strip}_{hit} = (i-1) \times n + j, \tag{1}$$

where i is the index of the ***StripSet*** and the j is the index of the ***GroupSet*** corresponding to the crossing position; n is the number of adjacent fibres in a *GroupSet*. The total number of fibres in a x, or y, layer is n times the number of the *GroupSet*.

The same formula is used to calculate the x and y coordinates. In the PSD, the total number of fibres per layer is 160, divided by four for the *GroupSet*. To reduce fibre length and overall detector size, instead of reading each fibre from both ends, two layers of fibres, one for the *GroupSet* and one for the *StripSet* are used. In this way, both x and y planes are made by superimposing two

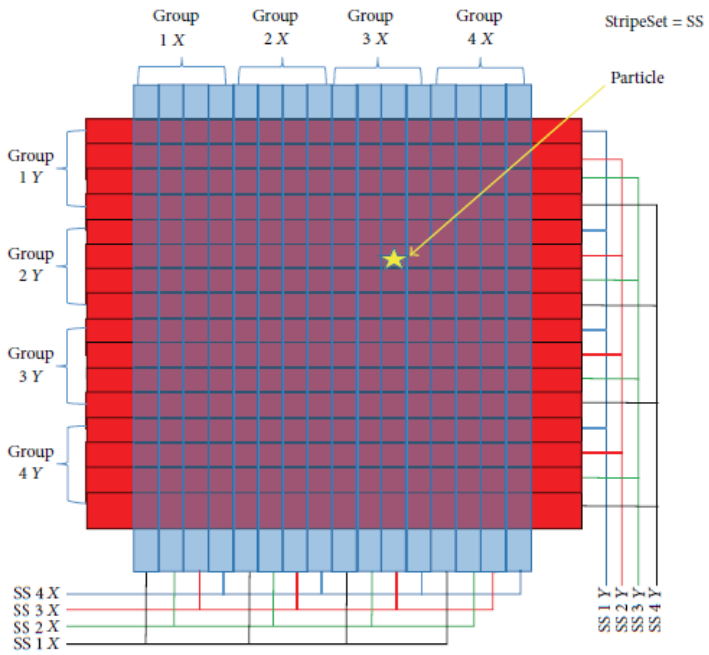

Figure 3: Diagram of the channel reduction system for a position sensitive detector composed of 16 by 16 fibres. The star is the particle crossing point in the sensitive area constituted by the area under the superimposition of the two layer of fibres.

aligned fibre layers.

4. The PSD DAQ chain

The output signals from the SiPM are sent for processing to an electronic acquisition chain, organised into two main levels. The first level consists of front-end electronics where analog-to-digital signal conversion takes place. The digital output signals of the front-end are fed into a National Instrument System-on-Module (NI SoM) [10] for decoding and filtering. This device is interfaced via gigabit Ethernet to a PC, which displays filtered data in real-time and stores raw data (unfiltered) for further analysis.

4.1. The PSD Front-end electronics

Two identical front-end boards for each, X and Y, direction process the corresponding SiPM signals. This custom designed board houses a 64 channels SiPM array, amplifies and filters the analogue signals and compares each to an individual threshold, remotely settable by a DAC, by means of an array of fast comparators. The individual threshold is necessary to compensate for the lack of uniformity of the different SiPMs and optical couplings between the SiPM and fibres. Each board provides 56 bits which represent the status of the SiPM signals.

4.2. The PSD Read-out and DAQ electronics

The logic signals produced by the comparators are sampled at high frequency, 250 MHz, by the SoM Field Programmable Gate Array (FPGA). This data is transferred to the SoM processor via Direct Memory Access (DMA). The processor applies real-time filtering algorithms and reconstructs the particle's point of impact, after discarding any spurious events. The NI SoM [10] is a fully tested and validated device with a complete middleware solution and an NI Linux Real-Time Operative System. It is based on a microprocessor with RAM, input/output ports, and all the other features that make it equivalent to a functional computer on a single board. These devices also incorporate an FPGA, an integrated circuit that can carry out very complex logic functions. The NI SoM uses a graphical approach, by means of the LabVIEW [11] platform for FPGA programming. A dedicated processor handles the SoM's input and output via a gigabit Ethernet connection to the acquisition PC. The LabVIEW platform also manages the entire acquisition chain and data processing in real-time.

5. The residual range detectors (RRD)

As for QBeRT, the RRD prototype is an upgrade of previous systems with some innovative solutions to optimise performance.

5.1. The operating principle of the RRD

The RRD prototype consists of a stack of 60 layers 9×9 cm^2 wide. Each layer is a ribbon of 500 µm square SciFi BCF-12 aligned, juxtaposed and oriented horizontally. The light produced within the ribbons by the passage of the particles is collected at both ends of the ribbon by means of 1 mm square Wavelength Shifting (WLS) fibres which are optically coupled to SiPM, one for each layer of RRD, to detect the collected light in the corresponding layer. The SiPM array sensor (Hamamatsu Photonics, mod.S12642-0808PB-50) is identical to those used for the PSD. The electronics for the RRD read-out and data acquisition is already described in the PSD section. However, only one SiPM array and one front-end board are used for the RRD.

The main advantage in using scintillating fibres is that the scintillation light is channelled into the fibre so it can directly reach the WLS fibre where it is trapped and guided to the SiPM. Because the re-emission of scintillation light is isotropic, only a small fraction of light in a plate of plastic scintillators can reach the WLS fibre. So, to obtain a sufficient number of detectable scintillation photons, the thickness of the scintillation plate (typically a few millimetres) should be increased. In our solution, the scintillating plane thickness equals that of the fibres thus improving range resolution by increasing the number of bins into which the RRD is divided.

A proton crossing the RRD, passes through a number of layers proportional to its input energy, before stopping. The dose released by the proton in each layer has an inverse profile, which increases with depth up to the Bragg peak which is the layer in which protons produce more scintillation light corresponding roughly to the point where they stop in the medium. After calibrating the response to the energy deposited in the detector, which means obtaining a relation similar to $R_0 = \alpha E_0^p$ [12], the particle's initial energy can be measured by observing the layer in which it deposits the higher dose. During the design phase, a series of prototype response simulations were carried out. The maximum measurable range was 36 mm in polystyrene/PVC and this was enough to stop protons with 67 MeV input energy.

5.2. Description of the prototype

A picture of the prototype during the assembly phases is shown in figure 4 where it is resting on its front. The WLS fibres corresponding to each RRD layer are clearly visible. The various layers are fixed and aligned with an aluminium support, which guarantees the detector's mechanical stability. Each ribbon layer is enclosed in a plastic frame built by a 3D printer. In figures 5(a) and 5(b), the frame is visible, and the layer is fixed to this frame by means of double-sided adhesive tape. On the lower side of the frame there is a groove (5(d)) on which the WLS fiber is fixed to the support by double-sided adhesive tape.

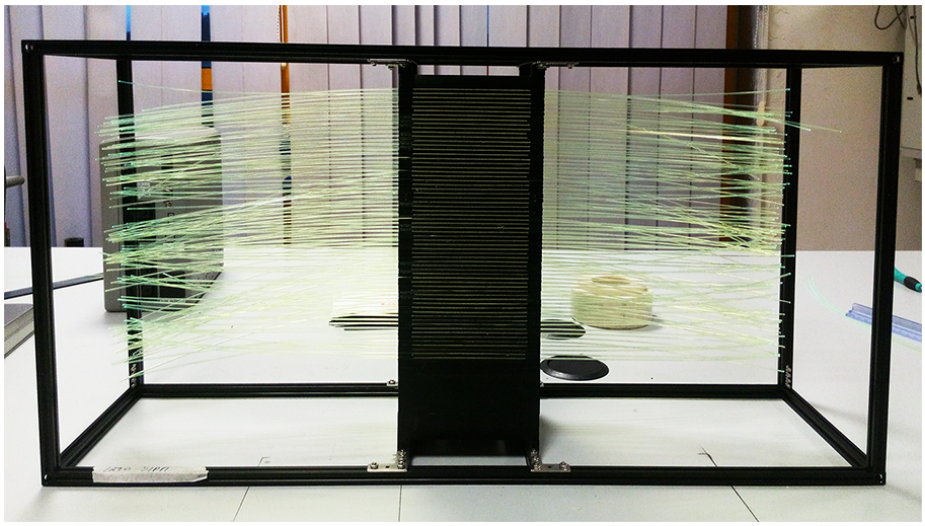

Figure 4: Side view of the RRD prototype during assembly.

The SciFi ribbon and WLS fibres are optically coupled by placing one side of one WLS fibre onto each of the two ribbon ends. To avoid optical cross-talk between two adjacent layers which would degrade range resolution and therefore energy measurement, each layer is optically isolated from the others by means of 100 µm thick black adhesive film. This film covers only one side of the layer, as seen in figure 5(d). Unlike in the PSD, the RRD SciFi have no optically insulating layer of EMA. So, any optical cross talk between adjacent fibres does not affect detector resolution.

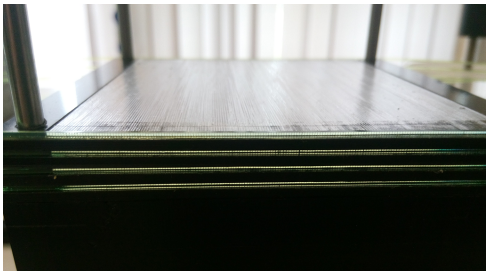

(a)

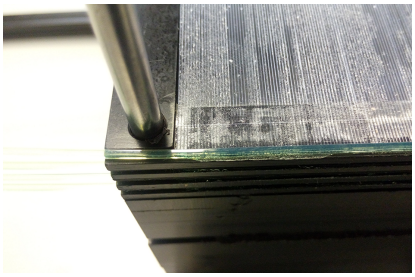

(b)

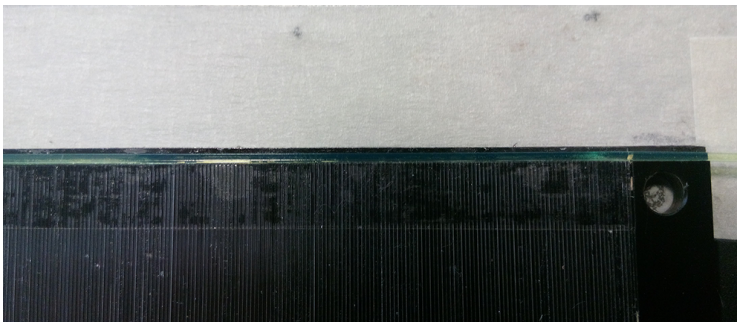

(c)

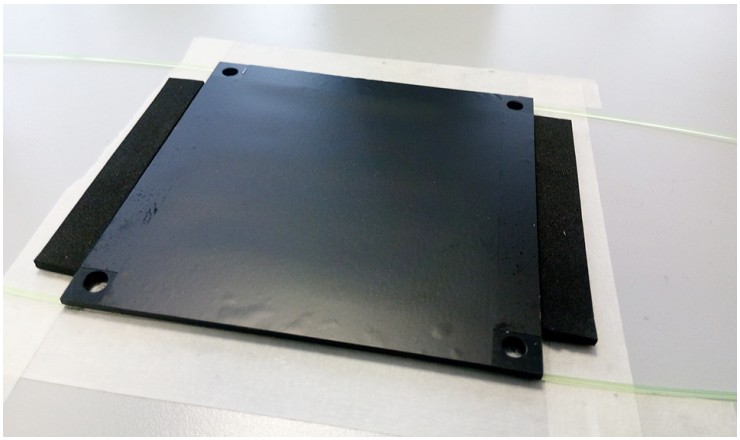

(d)

Figure 5: Different views of the RRD layers during assembly.

5.3. WLS-SiPM optical coupling

A fraction of the scintillation light produced in the SciFi is channelled into the fibres and propagates towards the WLS fibres, which, after absorption and re-emission, guide the light to the photo-sensor. After being trapped in the WLS fibre, the scintillation light can propagate towards the two opposite free ends of each fibre (see figure 5). The WLS fibres are read-out at both ends. Therefore, two SiPM arrays with different read-out strategies can be used. In the acquisition phase, observing the signal of one SiPM module or both can be decided to compensate for eventual malfunctions or non-uniformity in the WLS fibres/SiPM optical coupling. Both ends of the WLS fibres of each layer are optically coupled to the same channel of the SiPM array, creating a correspondence between the channel and the RRD layer. In this way, only 60 channels for each side of the detector are required, coupled to the 64-channel SiPM array.

5.4. The RRD electronics

An electronic chain, identical to that described in the previous section, processes the electrical signals produced by the SiPM array. The only difference resides in the data acquisition software.

6. The test strategy

Measurements at the CATANA proton therapy facility were carried out to validate and characterize the performance of the prototypes. There, a superconducting cyclotron is able to accelerate protons up to a maximum energy of 62 MeV. In the treatment room, the proton beam emerges from a metal pipe with a maximum energy of 58 MeV. The transverse dimensions of the beam can be adjusted with collimators placed at the end of the beam pipe. The first part of the beam test verified the response of the RRD detector. A cylindrical collimator with inner diameter of 2.5 cm was applied to the pipe. The proton beam crossed the QBeRT PSD and was stopped in the RRD. The beam energy was modulated by placing a different calibrated range shifter prior to the pipe.

The nominal RRD input energy and the corresponding standard deviations were calculated by means of SRIM (Stopping and Range of Ions in Matter), a group of programs for the calculation of the ion range (up to 2 GeV/amu) in matter [13] and are reported in Table 1.

Range Shifter	**Composition**	**Thickness** [mm]	**RRD Input Kinetic Energy** [MeV]	σ [MeV]
Beam Energy			53.86	0.19
A0	PMMA	0.50	53.16	0.23
A2	Al	0.95	51.47	0.25
A5	PMMA	4.48	47.35	0.34
A7	PMMA	6.62	44.56	0.36
A10	PMMA	8.96	40.06	0.44
A12	PMMA	10.68	36.92	0.53
A15	PMMA	13.34	31.66	0.60
A17	PMMA	15.10	27.75	0.69
A20	PMMA	17.80	20.65	0.92
A22	PMMA	19.58	14.52	1.29

Table 1: Specifications of the calibrated range shifters employed in the measurements.

7. Simulations with SRIM

Monte Carlo simulations with SRIM evaluated prototype performance prior to the beam test and calculated proton ranges in the detector. SRIM is based on a quantum-mechanical treatment of collisions between ions (incident particles) and the atoms of the fixed target. In particular, TRIM (Transport of Ions in Matter) permits the building of different layered targets being able to calculate of the final distribution of ions in three dimensions and other configurations. The experimental apparatus was modelled as follows:

- The first layer represents the range shifter used to modulate the beam energy;

- A 1320 µm PVC layer and a 2000 µm polystyrene layer, respectively, model the PSD placed in front of the RRD;
- A 20 mm air layer, models the distance between the sensitive areas of the two detectors;
- The remaining layers, alternately 100 µm layers of PVC and 500 µm polystyrene, simulate the RRD.

The results of the simulations are summarized in Table 2. For each value of proton kinetic energy detected at the prototype RRD in Table 2, the corresponding values of the simulation range were reported in the figure 7 graph. The simulated range error is calculated as the square sum of the straggling and a priori resolution of the RRD ($600/\sqrt{12}$ µm). Data were fitted with the power law (2):

$$R = a + b\,E^{1.75}, \tag{2}$$

where R is the range of the protons in the RRD, E is the kinetic energy at the entrance of the RRD, a and b are free parameters of fit.

Range Shifter	**Range in RRD [µm]**	**Layer in RRD**
Beam Energy	23780 ± 372	40 ± 1
A0	23180 ± 363	39 ± 1
A2	21930 ± 370	37 ± 1
A5	18800 ± 670	32 ± 1
A7	16820 ± 601	28 ± 1
A10	13920 ± 384	24 ± 1
A12	12000 ± 387	20 ± 1
A15	9040 ± 390	15 ± 1
A17	7080 ± 405	12 ± 1
A20	4180 ± 420	7 ± 1
A22	2200 ± 1104	4 ± 2

Table 2: Results from the simulation of RRD response.

8. Strategy of data acquisition and analysis

When QBeRT PSD detects a particle, acquisition by the two detectors is triggered. PREDATE RRD measures range by exploiting the inverse dose profile of heavy charged particles, such as protons and carbon ions. When a particle passes through the various layers of the detector, in the Bragg peak zone, the deposited energy (ΔE) in one layer is much higher than the one deposited in the input layer region. The Time Over Threshold (TOT) of the SiPM signal is a rough estimation of the energy deposited in the layers by the particles, even in the non-linearity condition of the scintillator [14]. A suitable threshold setting can distinguish the layer signals corresponding to the Bragg peak. Figure 6 shows a histogram obtained from an RRD acquisition. It reproduces the detector's dose-depth profile, characterized by a distinct narrow peak ("Bragg peak") at the end of the particles' path. The Bragg peak position is not exactly at the very end of the particles' path but just prior. In this kind of application, it is an experimentally consolidated practice to assume the particle range measurement is where the intensity of the Bragg peak signal is at 10% of its maximum value. This point coincides with the layer on the right of the Bragg peak (or the next layer compared to the incident beam direction).

9. Test results

For each range shifter, i.e. for each settable beam energy, the range was evaluated as previously described. The range value distribution obtained from leading edge analysis is plotted in figure 7 and fitted by the power law (2). In this figure, the range values calculated from the simulation and corresponding power law fit are also reported. The resulting fit parameter values are shown in the figure legend. The data agrees well with the predicted trend described by eq.(2) and with the simulation values.

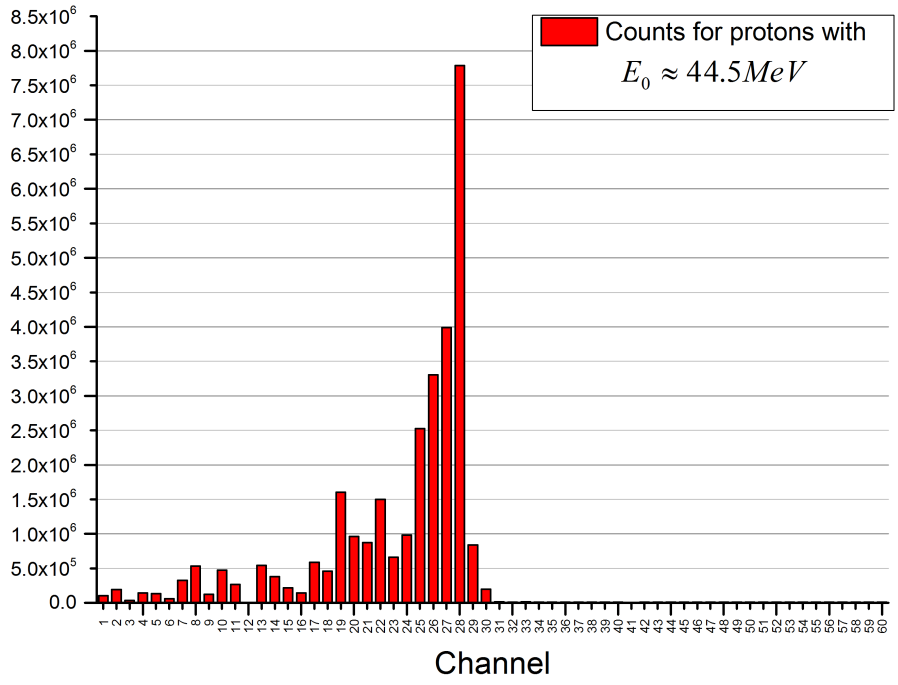

Figure 6: An example of histogram obtained from the RRD.

10. The QBeRT measurements

The second part of the test at CATANA was to validate the QBeRT prototype. The experimental set-up for the measurements was the same as described in the previous sections, the beam energy kept constant at 58 MeV.

10.1. Data acquisition and analysis

The PSD data acquisition strategy for imaging, was similar to that described for the RRD. To be detected, a particle should deposit enough energy in all the four fibre layers of the detector. When this condition is met, four read-out channels (one fibre channel and one ribbon channel for each direction X and Y) must generate a signal over the set threshold. In the case of the PSD, however, a logic high signal in any four channels is not sufficient to generate a trigger. So, due to dark current signals in SiPM arrays, in some channels, signals above the

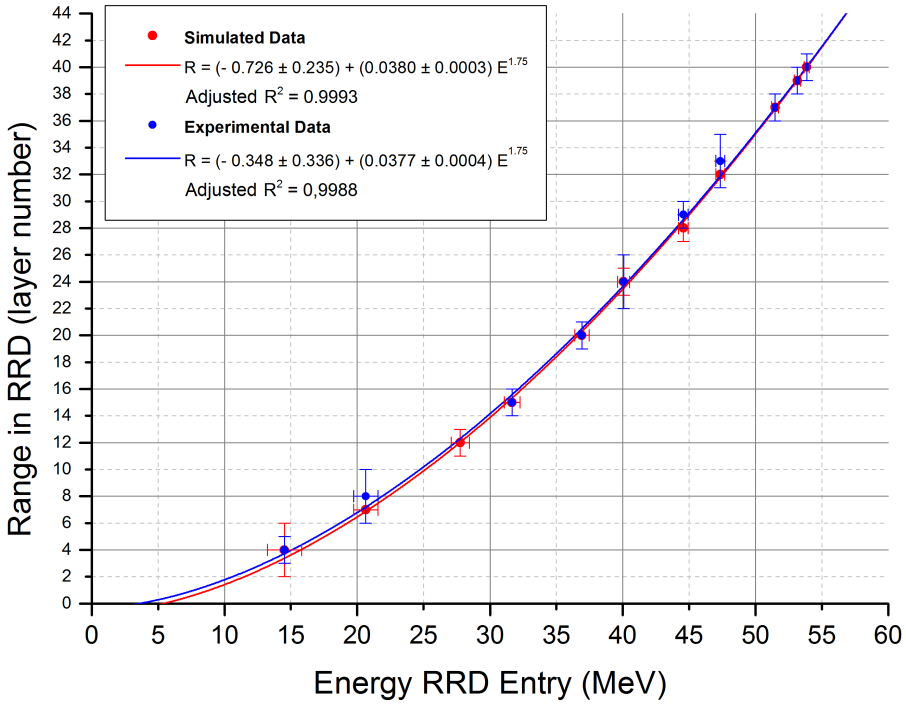

Figure 7: Comparison between the experiment and simulation data of the residual range with their respective fit.

threshold occur without any corresponding particle passage. This drawback is overcome in the acquisition phase by applying an appropriate algorithm which implements the quadruple time coincidence condition with a gate of two clock cycles: particle passage is associated with a signal above the threshold in two ribbon and two fibre channels within a narrow time interval. The acquired and filtered events are stored in a 160×160 matrix where each component contains the number of events in the corresponding pixel.

10.2. PSD resolution measurement

During the system test at CATANA, the PSD spatial resolution was experimentally characterised. A calibrated brass collimator with 1 mm diameter holes whose spacing increased from 1.5 to 1.9 mm per direction (figure 8(a)), was applied at the beam pipe exit. An image of this collimator was acquired by the

PSD and is shown in figure 8(b). From data analysis, the reconstructed hole centres can be estimated and compared with the projected collimator holes on the PSD. The results of this analysis are shown in figure 9. Then, the distances between the collimator hole centres and the reconstructed centres were calculated for each hole. The mean distance was about 130 µm, comparable with the (a priori) spatial resolution of the PSD, given by $500\,\mu m/\sqrt{12}$. This value takes into account all the effects due to small variations in fibre thickness and possible misalignment of the fibres.

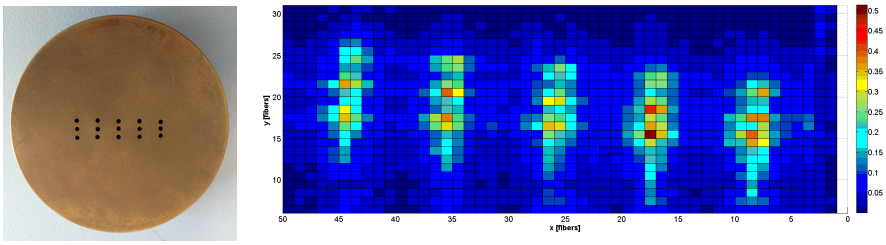

(a) (b)

Figure 8: Image of a calibrated brass collimator with 1 mm diameter holes, whose spacing increased from 1.5 to 1.9 mm per direction.

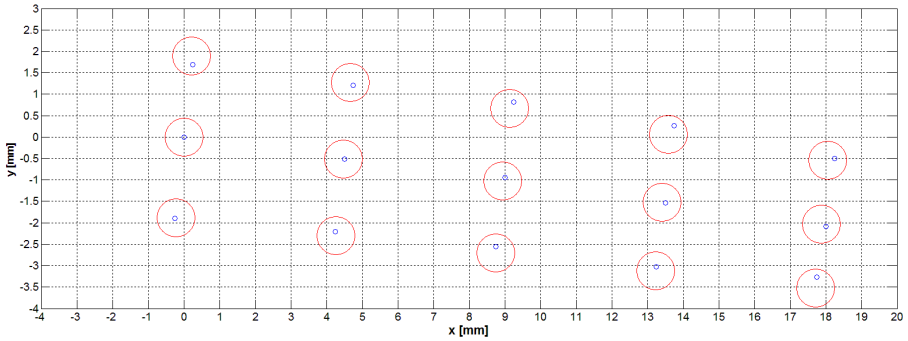

Figure 9: The red circles indicate the collimator hole projection on the tracker surface; the blue circles correspond to the hole centres reconstructed from the acquired image.

11. The proton radiography

The last part of the proton beam test at CATANA checked the performance of the two prototypes in radiography configuration. The experimental set-up (Figure 10) remained as previously described, but the two detectors were active at the same time.

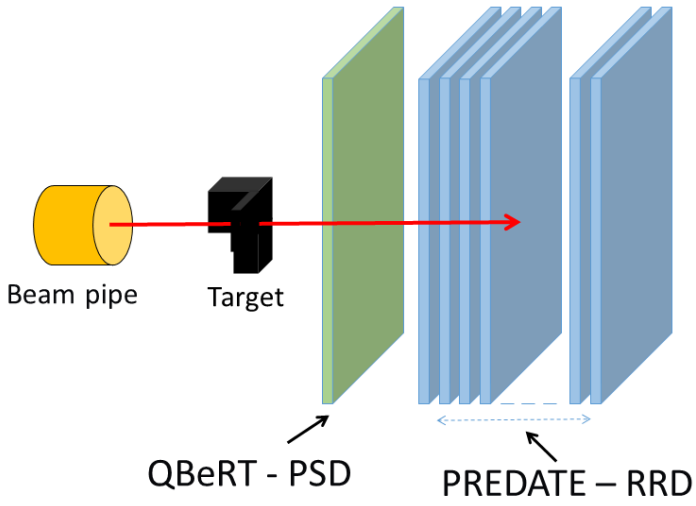

Figure 10: Test set-up for the radiography of the ladder target.

11.1. Data acquisition strategy and analysis

For a radiographic image, a range measurement must be associated to each particle crossing the PSD at a given position. So, data acquisition must run at low beam intensity (imaging conditions, about 10^6 particles per second on average). When a particle produces a quadruple time coincidence in the PSD, the crossing position within the sensitive area is reconstructed and a trigger signal is generated to acquire the RRD which measures the particle range. The software analysis maps the positions produced by the PSD to the corresponding range measurements. At the end of data acquisition for each pixel, the software analysis calculates the centroid of the Gaussian fit on the distribution of the range measurements corresponding to that pixel. This procedure is reasonable

because the distribution of the measured ranges is expected to be a normal distribution. Furthermore, it has the advantage of filtering the spurious coincidences due to dark currents in the photo-sensor. The result of this analysis is, therefore, a 160×160 matrix, as many as the PSD pixels, in which each component is given by the mean range measurement of the particles that have crossed the corresponding pixels. Note that with a single PSD, one must necessarily assume that the input and output particle crossing positions through the calibrated target coincide, or that they undergo negligible deflection traversing the medium. This is not completely true.

A simple PVC ladder target was designed as a radiography target. Having a homogeneous density, the radiography contrast is given only by the differences in thickness traversed by the protons. The radiography image shown in figure 11 was acquired with a 3.5 cm diameter beam and putting the A12 range shifter (PMMA, 10.68 mm thickness) prior to the beam exit.

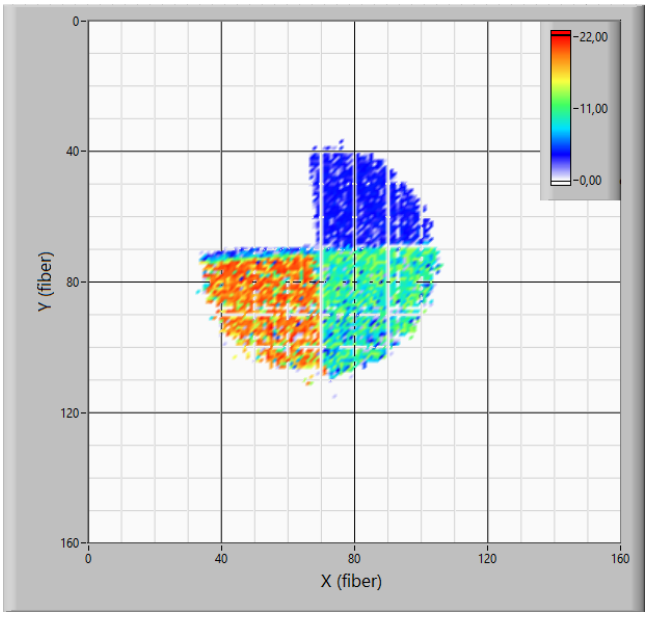

Figure 11: The radiography of the ladder target with A12 range shifter.

The colours in this image relate to average range measurements expressed

in numbers of RRD layers, pixel by pixel. It should be emphasised that the empty quarter-circle sector corresponds to the highest step of the ladder, with a thickness of 15 mm. Consequently, the 58 MeV protons of the CATANA beam do not have sufficient energy to cross the overall thickness of the A12 range shifter + 15 mm of PVC. Furthermore, the radiography shows boundary effects due to the non-orthogonality of the ladder with respect to the beam and the inevitable divergence of the beam by using a range shifter. Generally, the empty radiography pixels are those where the range measurement count is low and those, therefore, have been filtered by the reconstruction algorithm. Many of these pixels are aligned along the same row or column, suggesting that the problem is due to low tracker efficiency in those areas. In figure 12(a) and 12(b), the radiography shows two different perspectives of a 3D plot.

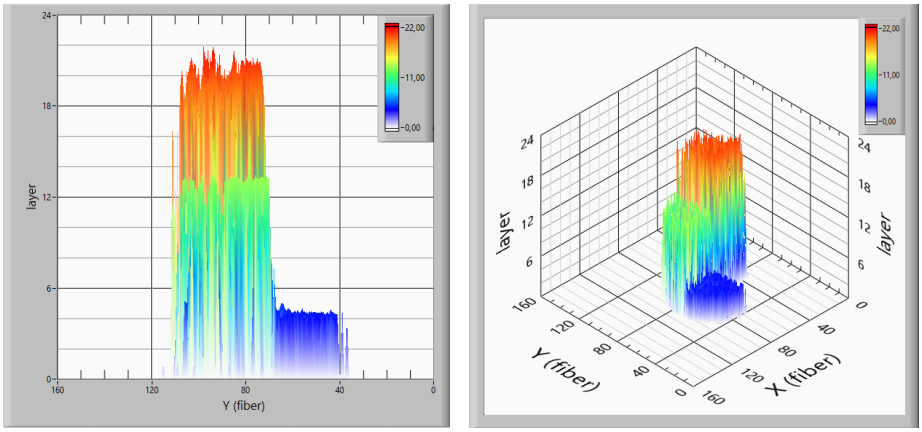

(a) (b)

Figure 12: Two different perspectives of the 3D representation of the radiography.

In fact, the interest in charged particle imaging lies in the energy released in the medium which can generate a map of electron density. Therefore, it is important to calculate the relation between the measured range and the ΔE energy lost by the particles. The evaluation of ΔE must also take into account the energy lost by the particles in the PSD, which is interposed between the ladder and detector to measure range. Since the sensitive areas of both detectors

are made of 500 µm layers of scintillating fibres, the PSD can be considered as the front of the RRD. The residual proton range in the PSD and RRD was simulated as a function of the particle incident energy in the tracker E. The range values thus obtained were fitted to the power law $R = A + B \cdot E^{1.75}$, where R is the particle range in the RRD and PSD, expressed in the number of layers, and the resulting fit parameters are $A = -0.191 \pm 0.311$ and $B = 0.0370 \pm 0.0006$ ($R - \text{square} = 0.998$). Therefore, the energy loss ΔE can be easily calculated as:

$$\Delta E \text{ [MeV]} = 58 - \left(\frac{R - A}{B} \right)^{1/1.75} . \tag{3}$$

The final radiography obtained after applying the energy-range conversion formula, is shown in figure 13.

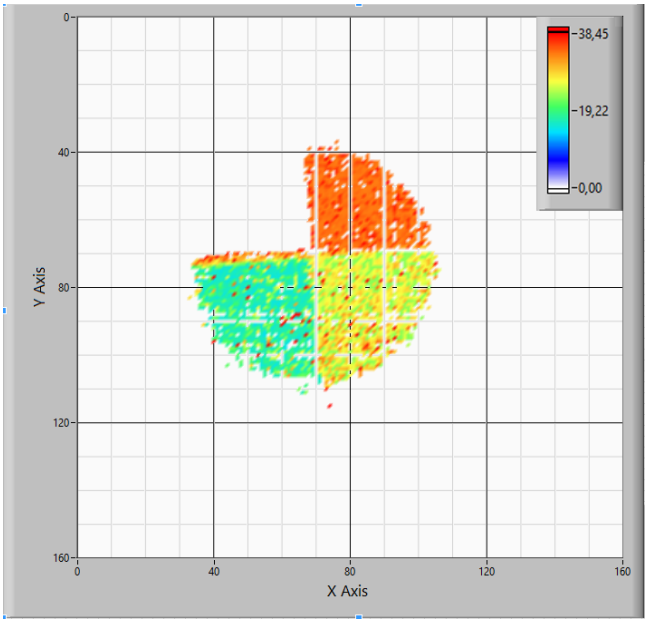

Figure 13: The radiography of the ladder with A12 range shifter expressed in energy loss.

12. TRIM simulations

To validate the radiographic images reconstructed from the measurements, two different groups of experimental set-up simulations were carried out using

the TRIM software. The first reproduced the protons crossing the A12 range shifter, the ladder, the PSD, and the RRD. The particle range values calculated by the software were converted into the number of layers crossed by the particle and suitably associated to a pixel to reproduce the beam spot size of 3.5 cm diameter. The final result is shown in figures 14. Figure 14(a) shows the three thickness areas of the ladder. They are much more homogeneous compared to the radiographic images of the measurements. This is because the TRIM software cannot simultaneously simulate a particle crossing volumes of different thickness.

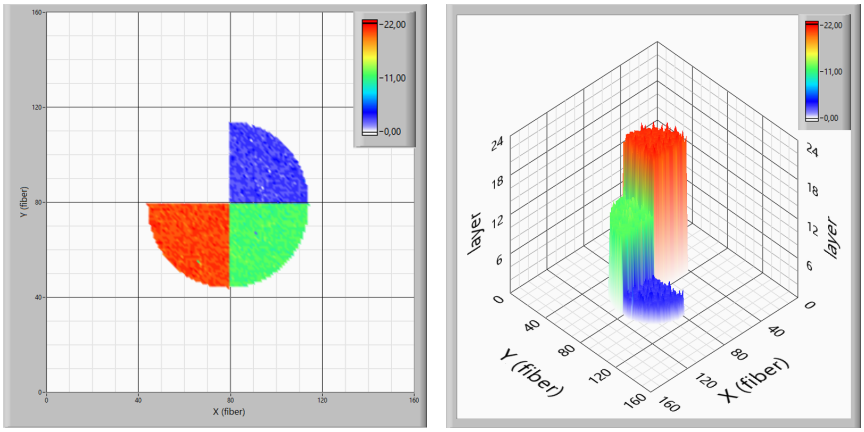

(a) (b)

Figure 14: 2D (a) and 3D (b) plot of TRIM simulation results for the radiography of the ladder post A12 range shifter, expressed in number of traversed layers.

The second group of simulations calculated proton residual energy after passing through the A12 range shifter and the different thicknesses of the ladder. By subtracting these values from the initial beam energy (58 MeV), the proton energy loss through the ladder could be calculated.

13. Energy loss to thickness conversion

The stopping power values S_i [MeV/mm] for the appropriate energy range were calculated with SRIM using energy intervals of 1 MeV, so the previous

equation can be rewritten as:

$$L(\Delta E)\,[\text{mm}] = \sum_{i=0}^{N} \frac{\Delta E_i}{S_i}, \tag{4}$$

$$\Delta E_i\,[\text{MeV}] = \begin{cases} \Delta E - i, & \text{if } \ 0 \leq \Delta E - i < 1 \\ 1, & \text{if } \ \Delta E - i \geq 1 \end{cases} \tag{5}$$

where $\Delta E = E_{in} - E_{out}$ is particle total energy loss and N is a positive integer such that $0 \leq \Delta E - N < 1$. The formula for the conversion of the energy lost in crossed thickness was applied to both the data matrix relative to figure 13 and to simulated values of ΔE. The resulting images are compared in figure 15.

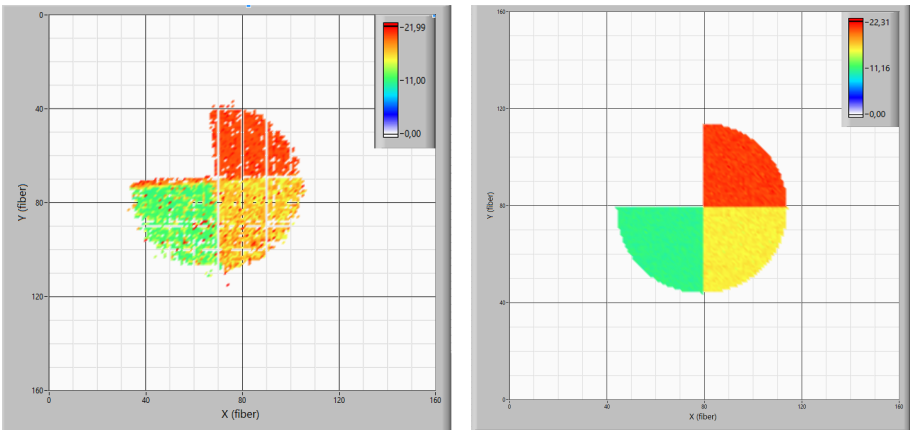

(a) (b)

Figure 15: Comparison between ladder radiography from measured data (a) and from simulated data (b).

14. Radiograph data analysis

As mentioned earlier, radiography images reconstructed from range measurements are subject to some limitations: (i) not knowing the effective paths of the particles crossing the phantom because only one PSD was used. In this case, particle trajectories according to the effect of Multiple Coulomb Scattering

cannot be corrected; (ii) the phantom wasn't placed at beam isocenter and perfectly perpendicular to the incident beam direction, which introduced further beam divergence. Therefore, appropriate data filtering of range measurements is necessary to reduce these effects when calculating the thickness of material crossed by the particles.

From the simulations, it is known that when protons with an initial energy of 58 MeV cross the A12 range shifter, phantom, tracker and stop in the RRD have a maximum range straggling of $\sigma_{str} = 0.4$ mm, which already includes the effects of initial energy spread (0.3 MeV). So, in a Region Of Interest (ROI) corresponding to a ladder step, a range of measurements around the expected value can be selected from the simulation plus or minus two layers (equal to $6\,\sigma_{str}$). A Gaussian fit was applied to all range measurement distributions obtained in this way and the results are shown in Table 3.

ROI		**Average Range** [no. of layers]	σ [no. of layers]
$67 \leq x \leq 97$	$40 \leq y \leq 70$	4.011	0.713
$75 \leq x \leq 105$	$75 \leq y \leq 105$	10.038	0.723
$30 \leq x \leq 70$	$70 \leq y \leq 110$	20.071	1.087

Table 3: Mean values and standard deviations (σ) of measured range in the specified ROI. The extensions of ROI are in number of fibres.

Subtracting the square of the maximum range straggling value of $\sigma_{\mathrm{str}} = 0.4$ mm from the standard deviation of range measurements, which already includes the effects of initial energy spread, it is again possible to find the a priori range resolution of about 170 µm.

These mean range values can be converted into proton energy loss and subsequently into crossed thickness using equations (3) and (4), to be compared with simulations. The results of average thickness calculation are shown in Table 4. Table 5 reports the values obtained from the simulations in the corresponding ROI.

ROI		Average Thickness [mm]	σ [mm]
$67 \leq x \leq 97$	$40 \leq y \leq 70$	20.158	1.504
$75 \leq x \leq 105$	$75 \leq y \leq 105$	16.699	1.362
$30 \leq x \leq 70$	$70 \leq y \leq 110$	10.899	1.520

Table 4: Mean values and standard deviations (σ) on the thickness calculated from measurements calculated in the specified ROI. The extensions of ROI are in number of fibres.

ROI		Average Thickness [mm]	σ [mm]
$83 \leq x \leq 108$	$83 \leq y \leq 108$	20.820	0.31
$79 \leq x \leq 119$	$39 \leq y \leq 79$	15.819	0.27
$39 \leq x \leq 79$	$39 \leq y \leq 79$	10.703	0.27

Table 5: Mean values and standard deviations (σ) on the thickness calculated from simulations in the specified ROI. The extensions of ROI are in number of fibres.

15. Conclusions

This paper presents the design and characterization of an innovative imaging system for charged particles based on Scintillating optical Fibres (SciFi). The system consists of a Position Sensitive Detector and a Residual Range Detector. Both prototypes, with a sensitive area of 9×9, cm^2, have innovative features which distinguish them from all other devices dedicated to these measurements. In addition, improvements in electronic chain acquisition and the use of SiPM arrays, in principle make the use of the PSD as a beam monitoring system possible, measuring the position, the fluence and the X-Y beam profiles. The verification of this feature will be investigated during the next beam tests.

The prototypes' performance was tested at the CATANA proton therapy facility (LNS) with energies up to 58 MeV. In addition, Monte Carlo simulations of the RRD detector response and the overall radiography system were carried out. From the test data analysis and by comparing simulations, the system architecture was validated.

Future tests at the hadron therapy centres of Pavia (CNAO, Hadron therapy

National Oncology Centre) and Trento (TIFPA, Trento Institute for Fundamental Physics Applications) should be able to validate the functionality of these devices with active beam shaping systems using protons with energies up to 250 MeV and carbon ions up to 480 MeV/u. The final goal is the real time measurement of a treatment plan and comparison of the results with those provided by the official dose delivery.

References

[1] Cirrone G, Cuttone G, Lojacono P, Lo Nigro S, Mongelli V, Patti I, et al. A 62 mev proton beam for the treatment of ocular melanoma at laboratori nazionali del sud-infn. Nuclear Science, IEEE Transactions on 2004;51(3):860–5.

[2] Schneider U, Pedroni E. Proton radiography as a tool for quality control in proton therapy. Medical physics 1995;22(4):353–63.

[3] Lo Presti D. Detector based on scintillating optical fibers for charged particle tracking with application in the realization of a residual range detector employing a read-out channels reduction and compression method. INFN, patent n. WO2013186798; 2013.

[4] Poludniowski G, Allinson N, Evans P. Proton radiography and tomography with application to proton therapy. The British journal of radiology 2015;88(1053):20150134.

[5] Presti DL, Bonanno D, Longhitano F, Pugliatti C, Aiello S, Cirrone GAP, et al. A real-time, large area, high space resolution particle radiography system. Journal of Instrumentation 2014;9(06):C06012.

[6] Lo Presti D, Aiello S, Bonanno D, Cirrone GAP, Leonora E, Longhitano F, et al. Offset: Optical fiber folded scintillating extended tracker. Nuclear Instruments and Methods in Physics Research Section A: Accelerators, Spectrometers, Detectors and Associated Equipment 2014;737:195–202.

[7] Lo Presti D, Bonanno DL, Longhitano F, Pugliatti C, Reito S, et al. Development of a real-time, large area, high spatial resolution particle tracker based on scintillating fibers. Advances in High Energy Physics 2014;2014.

[8] Spieler H. Semiconductor detector systems; vol. 12. Oxford university press; 2005.

[9] Lo Presti D, Russo GV, Leonora E, Aiello S, Randazzo N, Sipala V, et al. Characterization technique of sub-millimeter scintillating fibers. In: Nuclear Science Symposium and Medical Imaging Conference (NSS-MIC), 2011 IEEE. IEEE; 2011, p. 2104–8.

[10] National instruments - system on module. `http://www.ni.com/pdf/embedded/NI_System_on_Module_Flyer.pdf`; 2016.

[11] Labview system design software - national instruments. `http://www.ni.com/labview/`; 2016.

[12] Ulmer W, Matsinos E. Theoretical methods for the calculation of bragg curves and 3d distributions of proton beams. The European Physical Journal Special Topics 2011;190(1):1–81.

[13] Ziegler JF. Srim, the stopping and range of ions in matter, introduction. `http://www.srim.org/SRIM/SRIMINTRO.htm`; 2016.

[14] Zocca F, Pullia A, Bazzacco D, Pascovici G. A time-over-threshold technique for wide dynamic range gamma-ray spectroscopy with the agata detector. IEEE Transactions on Nuclear Science 2009;56(4):2384–91.